Author/s:
Xie, K;Fu, Q;Chen, F;Zhu, H;Wang, X;Huang, G;Zhan, H;Liang, Q;Doherty, CM;Wang, D;Qiao, GG;Li, D

Title:
Controlling the Supramolecular Architecture Enables High Lithium Cationic Conductivity and High Electrochemical Stability for Solid Polymer Electrolytes

Date:
2024-04-25

Citation:
Xie, K., Fu, Q., Chen, F., Zhu, H., Wang, X., Huang, G., Zhan, H., Liang, Q., Doherty, C. M., Wang, D., Qiao, G. G. & Li, D. (2024). Controlling the Supramolecular Architecture Enables High Lithium Cationic Conductivity and High Electrochemical Stability for Solid Polymer Electrolytes. Advanced Functional Materials, 34 (17), https://doi.org/10.1002/adfm.202315495.

Persistent Link:
https://hdl.handle.net/11343/340253

ADVANCED FUNCTIONAL MATERIALS
www.afm-journal.de

Controlling the Supramolecular Architecture Enables High Lithium Cationic Conductivity and High Electrochemical Stability for Solid Polymer Electrolytes

Ke Xie, Qiang Fu, Fangfang Chen,* Haijin Zhu, Xiaoen Wang, Gongyue Huang, Hualin Zhan, Qinghua Liang, Cara M. Doherty, Dawei Wang, Greg G. Qiao, and Dan Li**

Solid polymer electrolytes (SPEs) are long sought after for versatile applications due to their low cost, light weight, flexibility, ease of scale-up, and low interfacial impedance. However, obtaining SPEs with high Li^+ conductivity (σ_+) and high voltage stability to avoid concentrated polarization and premature capacity loss has proven challenging. Here a stretchable dry-SPE is reported with a semi-interpenetrating, supermolecular architecture consisting of a cross-linked polyethylene oxide (PEO) tetra-network and an alternating copolymer poly(ethylene oxide-*alt*-butylene terephthalate). Such a unique supermolecular architecture suppresses the formation of Li^+/PEO intermolecular complex and enhances the oxidation stability of PEO-based electrolyte, thus maintaining high chain segmental motion even with high salt loading (up to 50 wt%) and achieving a wide electrochemical stability window of 5.3 V. These merits enable the simultaneous accomplishment of high ionic conductivity and high Li^+ transference number (t_+) to enhance the energy efficiency of energy storage device, and electrochemical stability.

1. Introduction

Solid-state electrolytes are essential for the development of solid-state electrochemical and ionotronic devices. Apart from chemical stability, many emerging flexible ionotronic systems such as electrochromic devices,[1] ionotronic-based actuators,[2] loudspeakers,[2] artificial skins,[3] touch pads,[4] and electromechanical transducers[5] require electrolytes with high ionic conductivity, sufficient mechanical performance and even high transparency, and particularly to maintain high ionic conductivity when undergoing repetitive mechanical deformations.[6,7] Dry solid polymer electrolytes (dry-SPEs) have long been pursued to address safety concerns and improve energy density.[5,8] Important criteria for dry-SPEs include[9] ionic conductivity, lithium transference number, electrochemical stability, and mechanical robustness. However, it has remained a great challenge to realize a combination of all these desirable properties in one electrolyte.

Over the past 15 years, SPEs have experienced a renaissance due to their affordability, lightweight nature, flexibility, ease of scale-up, and low interface impedance. The most prominent example of SPE is polyethylene oxide (PEO), which is capable of dissolving lithium salts through the coordination of Li^+ with ethylene oxide (EO). It transports Li^+ through segmental motion, which is enabled by its low glass transition temperature (T_g).[10,11] The ion migration in a PEO-based SPE was believed to occur mainly in the amorphous region of the PEO matrix,[9] governed by the

K. Xie, H. Zhan, Q. Liang, G. G. Qiao, D. Li
Department of Chemical Engineering
The University of Melbourne
Parkville, Victoria 3010, Australia
E-mail: dan.li1@unimelb.edu.au

Q. Fu
School of Civil and Environmental Engineering
University of Technology Sydney
Ultimo, New South Wales 2007, Australia
E-mail: Qiang.Fu@uts.edu.au

The ORCID identification number(s) for the author(s) of this article can be found under https://doi.org/10.1002/adfm.202315495

DOI: 10.1002/adfm.202315495

F. Chen, H. Zhu, X. Wang, G. Huang
Institute for Frontier Materials
Deakin University
Geelong, Victoria 3217, Australia
E-mail: fangfang.chen@deakin.edu.au

F. Chen, H. Zhu, X. Wang, G. Huang
ARC Centre of Excellence for Electromaterials Science
Deakin University
Burwood, Victoria 3125, Australia

C. M. Doherty
Commonwealth Scientific and Industrial Research Organization (CSIRO)
Private Bag 10, Clayton South, Victoria 3169, Australia

D. Wang
School of Chemical Engineering
The University of New South Wales
Sydney, NSW 2052, Australia

Vogel–Tammann–Fulcher (VTF) theory. That is, increasing the Li^+ concentration[12–14] and diffusivity (by lowering the T_g of the matrix[15]) is favorable for the ionic conductivity of SPEs at a given operating temperature. However, when more dissociated ions ("free" ions) are introduced into a conventional PEO-based SPE by increasing the salt loading, the T_g of the matrix increases. This is because the introduction of "free" ions leads to the formation of an intermolecular complex with EO units,[16–18] which in turn restricts the segmental motion[19] and results in a relatively low ionic conductivity of $\approx 10^{-5}$ S cm^{-1} at room temperature.[20,21] Therefore, for lithium salts in PEO-based SPEs, the optimal molar ratio of Li to EO typically ranges from 0.03 to 0.12.[18,22–29] Meanwhile, the counter anions from lithium salt are typically more mobile than Li^+, resulting in a low Li^+ transference number (t_+), mostly <0.3.[20] Increasing the lithium salt loading can improve t_+,[9] however this in turn degrades ionic conductivity and offsets the benefits of higher t_+. Another challenge is the lack of electrochemical stability for high-voltage applications (i.e., >4 V). This is mainly attributed to the presence of unstable lone electron pairs on the ether oxygen atoms along the PEO chains.[30]

Significant progress has been achieved in the development of new SPEs, involving techniques such as blending, cross-linking, compositing, or complexing.[11,25,31–35] For instance, tetra-PEO is an emerging family of cross-linked polymer networks composed of symmetrical constitutional PEO segments with narrowly distributed lengths and tetra-branched cross-linking junctions.[36,37] Tetra-poly(vinyl alcohol ether) has the potential to offer improved mechanical properties compared to conventional PEO networks formed through random cross-linking. This is because the homogeneous polymer network promotes an even distribution of the mechanical stress.[29,38,39] It has been reported that the tetra-PEO SPE prepared by the Michael addition reaction exhibits improved ionic conductivity and mechanical properties.[29,40] However, their t_+ is 0.23, which is at a similar level to other PEO-based SPEs.[11,41] Nevertheless, we saw this as an opportunity to create a PEO-based SPE with an optimal microarchitecture, rather than focusing on molecular-level chemical structures.

In this work, we develop a new class of SPE by introducing an alternating copolymer (Poly Active) into a tetra-PEO network to form an amorphous, transparent, and stretchable semi-interpenetrating network. The resulting polymer matrix can accommodate an unusually high concentration of lithium salt, up to 50 wt% ([Li]:[EO] = 0.18), without significantly affecting the T_g (←40 °C). The experimental and simulation studies reveal that the tetra-PEO can promote lithium salt dissociation while suppressing the formation of Li^+/PEO intermolecular complexes even at a high charge carrier concentration, thereby facilitating rapid Li^+ migration via intra-chain hopping; and the incorporation of Poly Active can substantially enhance the electrochemical and mechanical stability of the SPEs. As a result, the semi-interpenetrating tetra-PEO solid electrolyte (SITP) managed to achieve an ionic conductivity of $>10^{-4}$ S cm^{-1} and a t_+ of >0.5 along with an enhanced electrochemical stable window of >5.3 V at ambient temperature. This study demonstrates the great potential of developing high-performance SPEs by engineering the supramolecular architecture of existing polymer networks.

2. Results and Discussion

2.1. Synthesis, Physical Properties and Simulations of SITPs

In this study, we employed lithium bis(trifluoromethane sulfonyl)imide (LiTFSI) as the lithium salt to construct SPE due to its high dissociation constant. A series of semi-interpenetrating tetra-PEO (SITP) electrolytes was prepared by varying the mass ratio of the polymer precursors and LiTFSI. Their component and physical properties are summarized in **Table 1** and supplemented by Table S1 (Supporting Information) (Note S1, Supporting Information). The polymer matrix was crosslinked through a solid-state "click" reaction, as shown in **Figure 1a**. In a glove box, anhydrous tetrahydrofuran (THF) solution containing 4-arm PEO with thiol end-groups, PEO diacrylate, PolyActive, LiTFSI, and a photo-initiator 2,2-dimethoxy-2-phenyl acetophenone (DMPA) was cast on a smooth glass substrate. After the evaporating THF on a hot plate, the dried polymer film was cooled to R.T. and then exposed to UV irradiation (3.5 mW cm^{-2}). The UV-induced solid-state "thiol-ene" reaction exhibited an exceptionally high atomic efficiency. The acrylate groups of PEO diacrylate were converted to "S-C-C" bonds, as confirmed by the complete disappearance of the 'C═C' vibration in the Raman spectrum (Note S2 and Figure S1, Supporting Information). The significant decrease in the intensity of the "C—C/C═C" peak in the X-ray photoelectron (XPS) spectra of SITPs supports this conclusion (Figure S2, Supporting Information). Given the stoichiometric feeding ratio of thiol and acrylate groups (1:1), a nearly quantitative conversion of thiol groups indicates the successful formation of a homogeneous tetra-PEO network via a "thiol-ene" reaction.

The free-standing SITPs are flexible and highly transparent (Figure 1a). A 120 µm film of SITP can transmit 90% visible light (Figure 1b). The high transparency of SITPs also implies that the polymer matrix is highly amorphous and compatible with LiTFSI, even at a high salt concentration of 50 wt%. As seen from the FT-IR spectrum of the SITP-5 (Figure 1c), we observed the peaks at 1715, 1474, and 1456^{-1} cm, which are attributed to the C═O stretching of PolyActive and C—H bending of PEO, respectively. Except for the characteristic peak of LiTFSI, no new significant features appeared, indicating that the addition of the lithium salt had no noticeable effect on the chemical structure. High stretchability SPEs are the essential component of wearable devices in which mobile ions function. We incorporated PolyActive into the tetra-PEO network in order to further improve its mechanical properties and processability. We found that the resultant SITPs are transparent and flexible even when the weight content of LiTFSI is greater than that of tetra-PEO. Taking the SITP-5 (tetra-PEO/PolyActive/LiTFSI = 25/25/50 wt%, Table 1) as an example, this SITP exhibits a fracture strain of 146% (Figure 1d) and an elastic toughness of 764 kJ m^{-3}. In contrast, the uncrosslinked SITP-5 counterpart (Table S1, Supporting Information) displays a fracture strain of 57% and an elastic toughness of 236 kJ m^{-3}. The improved mechanical strength is contributed by cross-linking and introducing the intrinsically stretchable PolyActive (fracture strain = 209%; elastic toughness = 432 kJ m^{-3}).

In general, a lower T_g and a higher free charge concentration imply a higher Li^+ diffusivity, which is essential for enhancing the ionic conductivity of SPE. However, increasing Li^+

Table 1. Summary of the composition and physical properties of the prepared SITPs.

Entry	SITP composition				Properties		
	PolyActive [wt%]	tetra-PEO [wt%]	LiTFSI [wt%]	[Li]:[EO][a)]	Dissociation degree[b)]	[Li^+_{free}]:[EO][c)]	T_g [°C]
SITP-1	50	50	0	—	—	—	—
SITP-2	40	40	20	0.045	0.80	0.036	-42.7
SITP-3	35	35	30	0.078	0.77	0.060	-42.2
SITP-4	30	30	40	0.12	0.75	0.090	-42.3
SITP-5	25	25	50	0.18	0.63	0.11	-42.4
SITP-6	20	20	60	0.27	0.25	0.068	-44.6
SITP-7	30	20	50	0.18	0.62	0.11	-42.3
SITP-8	40	10	50	0.19	0.57	0.11	-41.2
cSPE-1	50	0	50	0.20	0.70	0.14	-47.4
cSPE-2	0	50	50	0.15	—	—	—

[a)] Total lithium to ethylene oxide unit (EO, -CH_2CH_2O-) ratio in mol: mol; [b)] The dissociation degree is defined as the ratio of dissociated lithium salt to the total lithium salt; [c)] The [Li^+_{free}]:[EO] = [Li]:[EO] × Dissociation degree.

concentration generally elevates the T_g of PEO-based SPEs because more dissociated Li^+ can form intermolecular complexes with EO units,[32–34],[19] which decreases the chain motion and subsequently Li^+ diffusivity.[42] This trade-off limits the lithium salt loading in the EO matrix for optimal ionic diffusivity (i.e., [Li]:[EO] <0.12, or [EO]:[Li] >8:1). Unexpected, the SITPs are capable of keeping consistent T_g ≈−42.5 ± 0.3 °C when increasing the [Li]:[EO] from 0.045 to 0.18 (Figure 1e–g; Figure S3 and Note S3, Supporting Information). As far as we know, this ratio is greater than that of conventional PEO-based, salt-in-polymer systems (i.e., [Li]:[EO] < 0.12) in the literature.[18,22–29] The SITP-6 with an even higher [Li]:[EO] shows a slightly decreased T_g of −44.6 °C, attributable to its incomplete cross-linking. In addition, we did not observe any PEO or PolyActive melting peaks in the DSC curves of the SITPs and the control samples (Figure S3, Supporting Information), indicating that a high amorphousness in the SITPs was achieved.[10] We further prepared a series of SPEs composted of linear PEO-based and LiTFSI and determined their T_gs using DSC (Note S4, Supporting Information). As shown in Figure S4 (Supporting Information), we observed a clear increase in T_g when increasing the LiTFSI concentration, which is in good agreement with previous reports.[43] Our first thought is that this result can be attributed to the introduction of Poly Active. Therefore, we performed XRD characterization of SITPs and observed a decrease in peak intensity in the XRD pattern, indicating that the introduction of Poly Active suppresses the crystallinity of PEO segments (Figure S5, Supporting Information).

We next measured the dissociation degree of LiTFSI in SITPs with the Raman shifts between 730 and 754 cm^{-1} as a key indicator of different $TFSI^-$ coordination environments [13] (Table 1, Figure 1f,g; Figure S6 and Note S5, Supporting Information). The dissociation degree gradually drops from 0.8 for SITP-2 ([Li]:[EO] = 0.045) to 0.63 for SITP-5 ([Li]:[EO] = 0.18). Despite the decrease in dissociation degree, the "free" Li^+ concentration ([Li^+]:[EO]) still increases from 0.036 for SITP-2 to 0.11 for SITP-5 due to the increase in salt concentration. While the [Li^+]:[EO] value drops to 0.068 for SITP-6 because of a significantly lower dissociation degree of 0.25 (Table 1). The data of T_gs and LiTFSI dissociation of SITPs are presented in Figure 1g for more intuitive analysis and comparison.

2.2. The Simulation Study on SITPs

We then utilized atomistic molecular dynamics (MD) with statistical correlation analysis to gain insight into the microstructure and dynamic aspects of a tetra-PEO network at the unusual high salt concentration of [Li]:[EO] = 0.18 (see details in SI2). The equilibrium system is a molecularly homogeneous amorphous phase with lithium ions uniformly distributed throughout the polymer matrix, as shown in a snapshot in **Figure 2**. Three different Li^+ coordination structures were identified and represented by different colors, corresponding to free Li^+ in PEO (Figure 2a, blue balls), Li-TFSI ion pair, (Figure 2b, green balls), and PEO-Li-TFSI complex (Figure 2c, pink balls) (Note S6, Supporting Information). The atomic percentage of Li^+ for free Li^+, Li-TFSI ion pair, and PEO-Li-TFSI complex structures were respectively determined 81%, 2%, and 17% (Figure S7, Supporting Information), supporting the high dissociation degree of LiTFSI, as revealed by Raman analysis. The MD simulations also suggest that most of the dissociated Li^+ coordinate with the oxygen atoms from the same PEO chain (Figure 2a–c), agreeing well with the observation in the correlation between T_g and salt concentration in SIPT-2 to −5.

The diffusion of Li^+ in different chemical environments was further investigated to reveal how the local structures affect Li diffusion (Figure 2d; Figures S9,S10 and Notes S7,S8, Supporting Information). We screened the fast and slow Li^+ according to their travel distance after a 6 ns MD production run. A snapshot in Figure S9b (Supporting Information) shows the distribution of fast and slow Li^+ in the polymer matrix, with the fast lithium appearing mainly in the middle of the PEO chains. The radial distribution function (RDF) was further calculated between the fast (or slow) Li^+ and the selected atoms in different structural environments, including the junction atoms, O atoms in the middle or at the end of a PEO chain, or in anions. A high coordination number suggests a high possibility of the fast or slow Li^+ present in this environment. This result suggests the formation

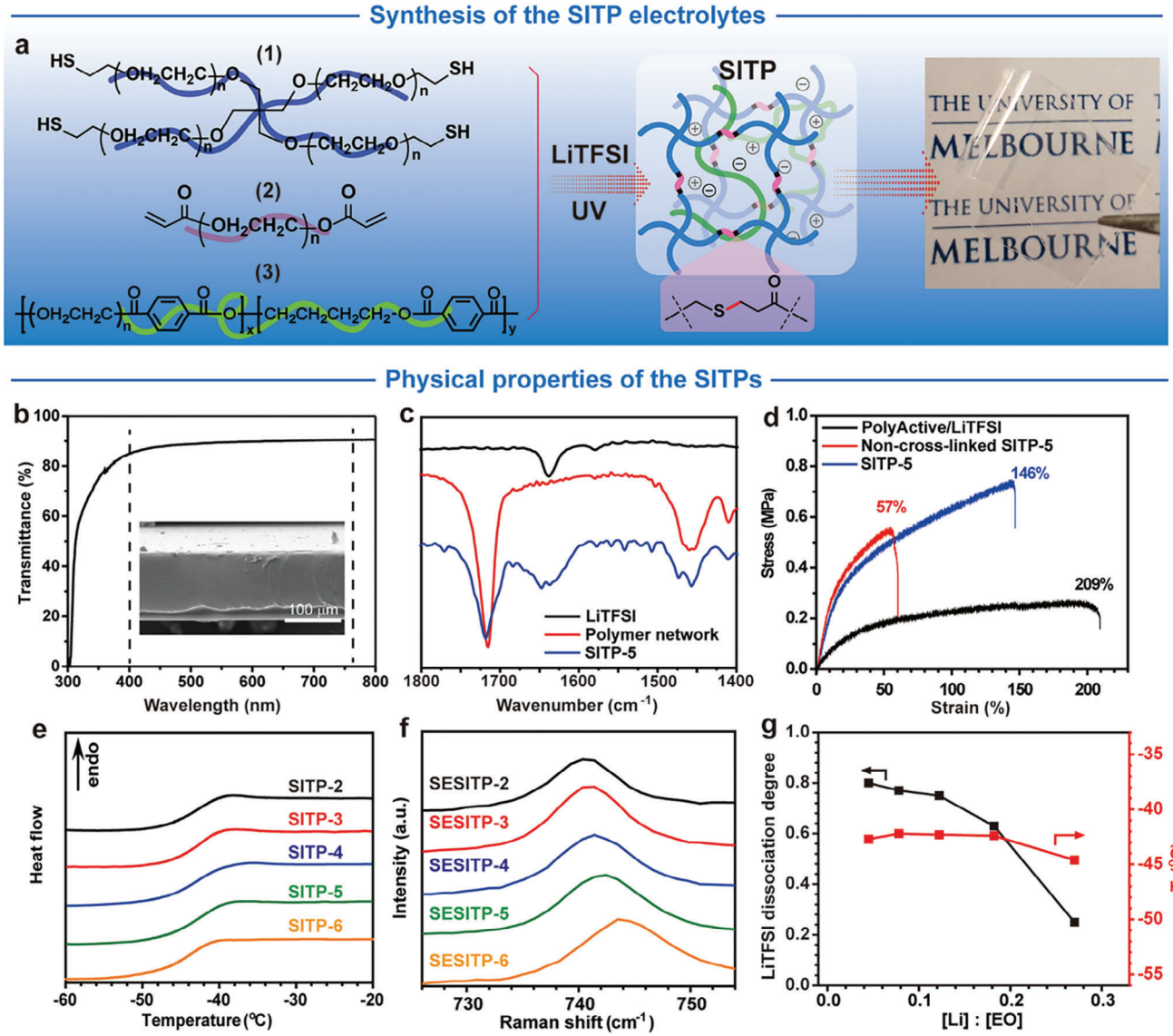

Figure 1. The fabrication and characterization of SITPs. a) Schematic illustration for the fabrication of SITPs, in this scheme: (1) is 4-arm PEO with thiol end-groups (MW = 5 kDa); (2) is linear PEO diacrylate (MW = 250 Da); and (3) is PolyActive. The digital photo shows the flexibility and transparency of a SITP film. b), Transmittance of SITP measured by UV–vis absorption spectroscopy. A SITP film with a thickness of 120 μm (insert chart) shows ≈90% transmittance in the visible light region (indicated by the dashed lines). c), FT-IR spectra of the LiTFSI, polymer matrix without salt and the SITP-5. d), Tensile stress–strain curves of dry-SPE samples: cSPE-1 ($PolyActive_{50}/LiTFSI_{50}$, black), SITP-5 ($PolyAcitve_{25}$/tetra-$PEO_{25}/LiTFSI_{50}$, blue), and the control SPE has the same composition as SITP-5, but without UV-induced cross-linking (red).

of Li-TFSI ion pairs is not favorable for Li^+ diffusion at room temperature. The fast Li diffusion in Li-TFSI clusters was only observed at higher temperatures (e.g., 120 °C). In all, both the experimental and computational results imply that the formation of the Li^+/PEO inter-chain complex (including near-junctions) that slows down the Li^+ movement is suppressed in the SITPs, allowing the accommodation of a high concentration of "free" charge carriers. Such a unique capability is one of the main promoters of the high ionic conductivity of SPEs.

The MD simulation was further performed on a linear PEO-based SPE[44] with the same LiTFSI concentration. We found that both Li^+ and $TFSI^-$ diffuse more rapidly in disconnected (linear) PEO than in cross-linked PEO networks, as indicated by the higher mean square displacement (MSD) of the former in Figure 2e. This result motivated us to investigate how the continuity of the tetra-PEO supramolecular architecture affects Li^+ diffusivity, especially in long-distance migration. As for an amorphous PEO-based SPE, varying the ratio of "inter-chain hopping" and "intra-chain hopping" will affect the ionic diffusivity for long-distance migration, as reported in recent studies.[19,45,46] In an inter-chain hopping model, Li^+ hops out of its original coordination shell completely, and the neighboring PEO chains need to have sufficient free oxygen coordination sites and be close enough

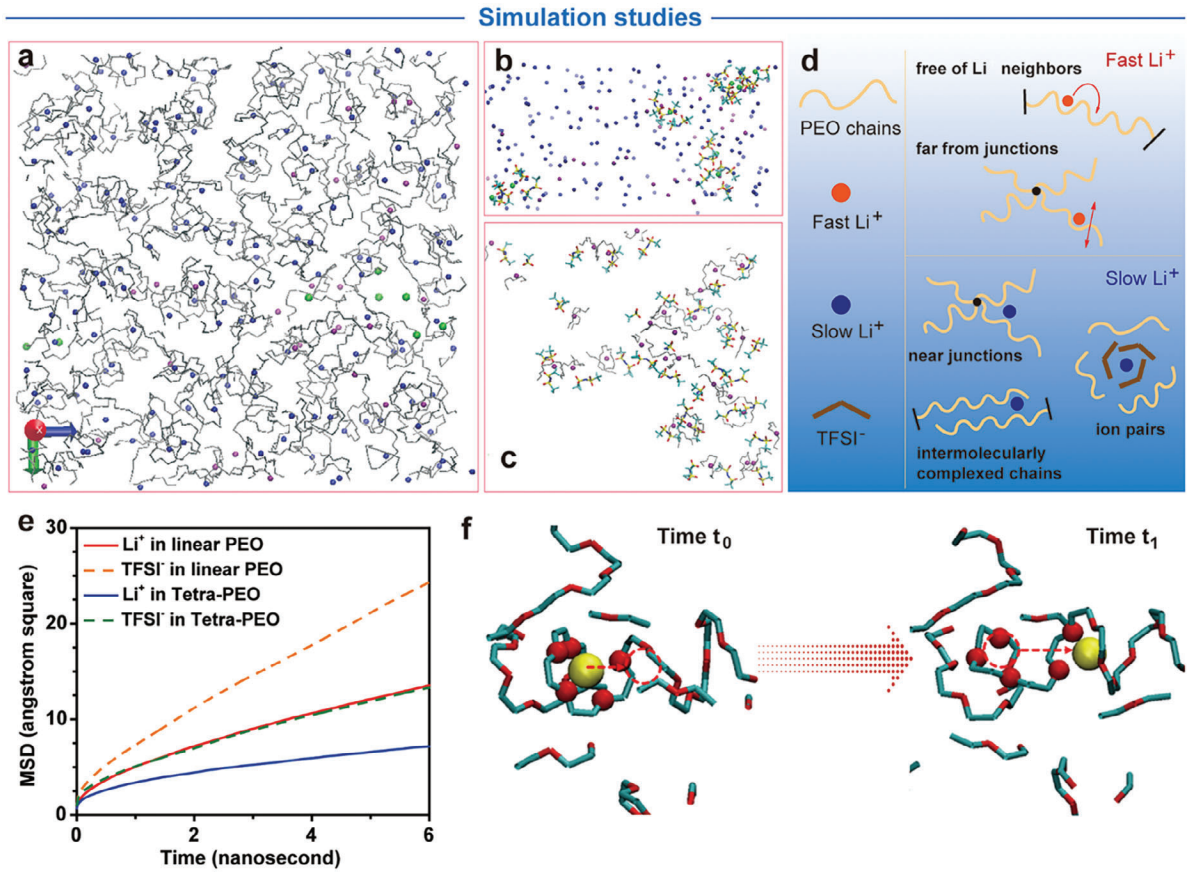

Figure 2. The MD Simulations of the atomic environments for the charge carrier in tetra-PEO. a–c), Snapshots to show Li^+ in different coordination states. Blue, purple, and green spheres refer to the Li^+ coordinated with only PEO, only $TFSI^-$, and both PEO and $TFSI^-$, respectively. Grey lines refer to PEO chains. $TFSI^-$ is not presented for clarity. d), Schematic of the atomic environment for fast and slow Li^+. e), Mean square displacement (MSD) of ions in linear PEO and Tetra-PEO with respect to simulation time. f), The lithium migration snapshot for an extended MD simulation period of 50 nm.

to capture the hopping Li.+[17] Such a transport mechanism requires much higher energy. In contrast, intra-chain hopping refers to the transport of ions along a single PEO chain through partially coordinating with new oxygen sites in the same chain.[19,45,46] This process can be promoted by a rapid motion of a polymer chain with low T_g and requires less energy than inter-chain hopping. In PEO-based SPEs, the ions transported via "inter-chain hopping" diffuse ≈20%–30% as fast as those via "intra-chain hopping" near room temperature.[19,45,46] Moreover, the MD simulation for 50 ns at 80 °C captures one to three Li^+ hopping events only through intra-chain hopping (Figure 2f and Supporting Video), suggesting that intra-chain hopping mechanism is more likely to be triggered at low temperatures from the perspective of the lowest energy consumption, which is also supported by other simulation studies.[9,17,44]

2.3. The Ionic Conductivity, Li^+ Diffusivities, Transference Number, and Electrochemical Stability Window of the SITPs

Next, we measured the ionic conductivity of the prepared SITPs. As shown in **Figure 3a**, the SITP-5 (with [Li]:[EO] = 0.18) exhibits a high ionic conductivity of 0.11 mS cm^{-1} at 30 °C and 1.03 mS cm^{-1} at 80 °C, which is comparable to the state-of-the-art solid electrolytes. We also found that an optimal content of Poly Active relative to the tetra-PEO network (approach 1:1 in weight) is necessary for achieving the maximum ionic conductivity of SITPs, regardless of the LiTFSI concentration (Figures S11,S12 and Note S9, Supporting Information detailed in SI3). While when we omitted the tetra-PEO, the ionic conductivities of PolyActive/LiTFSI SPE with 50 or 20 wt% LiTFSI are 8×10^{-4} and 1×10^{-4} mS cm^{-1} at 30 °C (Figure S12, Supporting Information), respectively, suggesting that the pristine Poly Active cannot facilitate rapid Li^+ transport. More controlled experiments were conducted to replace the tetra-PEO with linear PEO (M_n = 5 kDa) or randomly cross-linked PEO networks. These experiments revealed that the impact of Poly Active on ionic conductivity is also insignificant (Figure S13 and Note S10, Supporting Information).[47] In addition, we also incorporated Pebax 1657 into tetra-PEO as a guest polymer to replace Poly Active (Note S11, Supporting Information). The resultant SPE showed an ionic conductivity of 4×10^{-3} mS cm^{-1} at 30 °C (Figure S14, Supporting Information). These results, summarized in Table S2 (Supporting Information), suggest the importance of the co-existence of both PolyActive and tetra-PEO for achieving the high ionic conductivity of SITPs.

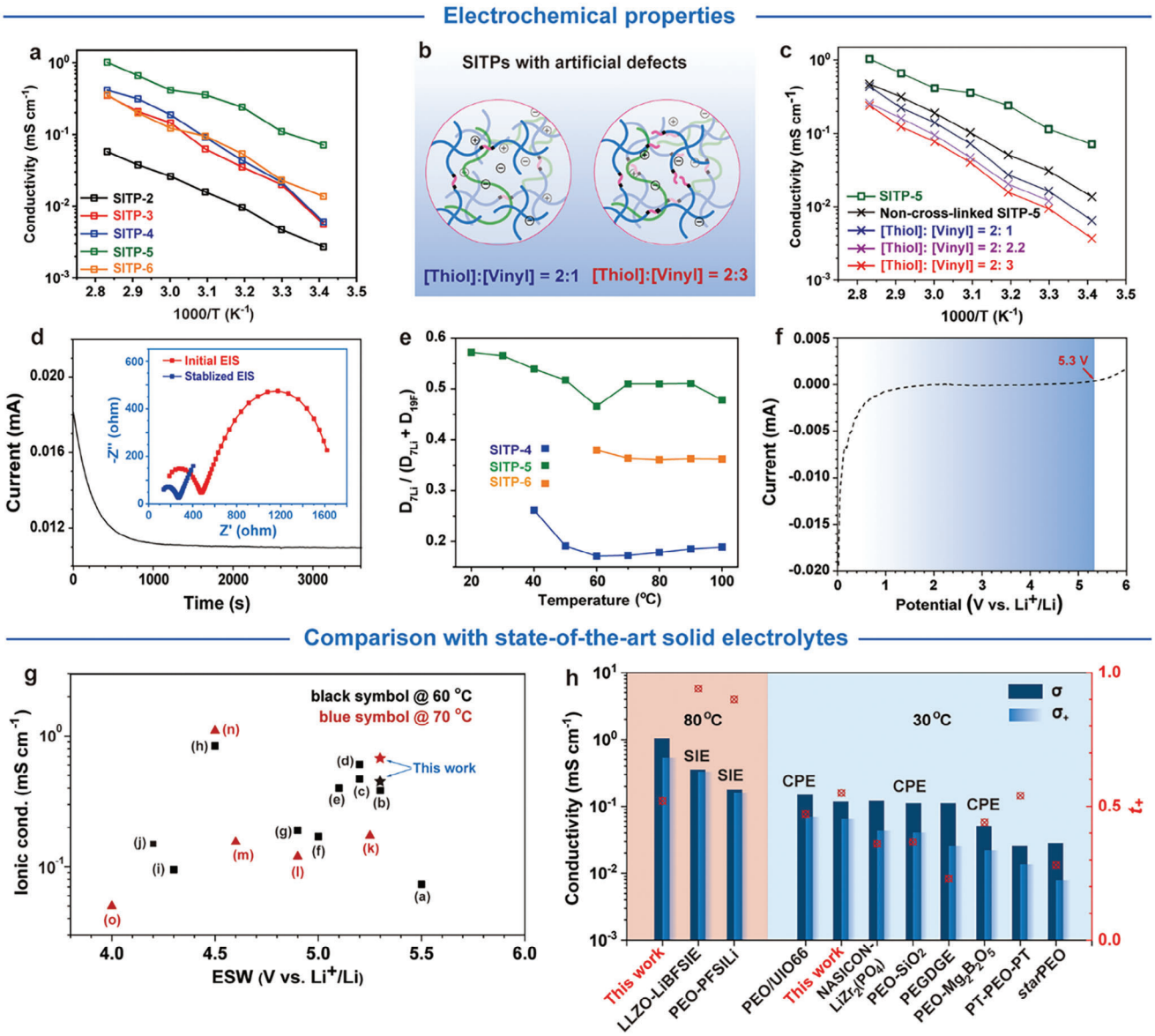

Figure 3. The electrochemical properties of the SITPs. a) The dependence of ion conductivity on temperature for SITPs. b) The schematic illustrations of the control SPEs with artificial structural defects. c) The ionic conductivities of dry-SPEs vary with temperature for the control SPEs. d) The measurement of electrochemical Li^+ transference number (t_+) for SESITP-5 using the following setup: [Li|SESITP-5|Li] and performing chronoamperometry with the voltage bias of 10 mV. The typical *I*–*t* curves and the EIS measurement on this setup before and after the steady state (insert). The average Li^+ transference number is determined to be 0.53. e) The contribution of D_{7Li} to total ion diffusion of D_{7Li} and D_{19F} measured by pulse-field gradient diffusion nuclear magnetic resonance (PFG-NMR) for SITP-4, SITP-5, and SITP-6 at different temperatures. f) The measurement of the electrochemical stability window for SESITP-5 by LSV method. g) Comparison of the ionic conductivity versus ESW of SITP-5 to the state-of-the-art solid electrolytes at elevated temperatures of 80 °C. Details of the comparison are included in Tables S3,S4 (Supporting Information). h) Comparison of the t_+ and Li^+ conductivity (σ_+) to the state-of-the-art solid electrolytes, including SPEs, single ion electrolytes (SIEs), and composite electrolytes (CPEs) at 80 °C and R.T.

Cross-linked tetra-PEO is known to exhibit improved mechanical stability than randomly crosslinked PEO networks.[39] However, in the conventional concept, cross-linking of the amorphous PEO chains will restrict the chain motion and elevate the T_g, thus decreasing ionic conductivity according to the VTF theory and previous works.[18,48–50] Indeed, the T_g of SITP-5 elevates from −51.9 (non-cross-lined tetra-PEO/PolyActive/LiTFSI, Table S2, Supporting Information) to −42.4 °C (Table S2, Supporting Information) after cross-linking. Intriguingly, the uncross-linked SITP-5 counterpart, despite having higher chain motion (see DSC data in Figure S3, Supporting Information), showed lower ionic conductivity, which was 3.5 times lower than that of the SITP-5. We then deliberately altered the stoichiometric ratio of thiol and vinyl groups ([thiol]:[vinyl] = 2:1 to 2:3) to introduce defects into SITP-5 (Figure 3b). The resultant SITPs with more structural defects show a significantly decreased ionic conductivity of over 90% than SITP-5 at 30 °C (Figure 3c). According to the physical properties, such as a lower T_g and higher

degree of dissociation, which generally affect ionic conductivity through VTF theory, it is expected that the SITP with a [thiol]:[vinyl] = 2:3 would exhibit higher or similar ionic conductivity compared to SITP-5. However, experimental data showed the opposite trend (Figure 3c; Table S2, Supporting Information). We speculate that the structural defects (beyond the molecular level) of SITPs can disrupt the migration path of Li^+ and increase the frequency of inter-chain hopping, thereby reducing the diffusivity of charge carriers over long distances. Combined with the above simulation study, we conclude that the continuity of the polymer network is one of the key factors in achieving high ionic conductivity, which has been overlooked in previous studies.

We reasoned that the major motivation for increasing lithium salt loading is to achieve a high Li^+ transference number (t_+). We thus evaluated the t_+ by electrochemical techniques using a [Li|SESITP-5|Li] setup (Figure 3d) and the pulse-field gradient diffusion nuclear magnetic resonance (PFG-NMR, Figure 3e).[14] The average t_+ is determined to be 0.53 through *I–t* and the EIS measurements. As shown in Figure S15 (Supporting Information) (Note S12, Supporting Information), The diffusion coefficients of ^7Li (D_{7Li}) of the SITP-5 ([Li]:[EO] = 0.18) are significantly higher than those of SITP-4 ([Li]:[EO] = 0.12) and SITP-6 ([Li]:[EO] = 0.27) in the whole temperature range tested. According to a previous report,[14] the apparent t_+ can be estimated by calculating the ratio of D_{7Li} to the total ion diffusion of D_{7Li} and D_{19F}. The PFG-NMR reveals that SITP-5 exhibits a high apparent t_+ of 0.57 at 30 °C and 0.51 at 80 °C (Figure 3e). This result can be attributed to the high LiTFSI loading and high salt dissociation degree,[14] which is consistent with the electrochemical measurements. In addition, we measured the fraction free volume (FFV) of SITPs by positron annihilation lifetime spectroscopy (PALS), and the results are shown in Figure S16 (Supporting Information) (Note S13, Supporting Information). As the [Li]:[EO] increased from 0.12 to 0.18, we observed a significant increase in FFV for SITP-5, which also contributes to the Li^+ diffusivity.

A wide potential window is attractive in electrochemical energy conversion and storage devices because this allows a high operating voltage, and consequently high energy density can be obtained. However, the oxidative stability of PEO-based SPEs is limited to ≈4 V due to the shielding of the positive charge in the polymer oxidized state by the salt anion. Reportedly, the addition of inorganic fillers can also enhance the electrochemical stability of PEO-based electrolytes. This effect has been observed in several types of fillers, such as SiO_2,[35] as well as lithium conductive fillers, like LAGP[51], and Garnets, such as LLZO and LLZTO.[52,53] As shown in Figure 3f, an anodic current was observed for the SITP-5 membrane. Considering the high PEO content of PolyActive (≈77 wt%, as disclosed in the Experimental Section), the resulting polymer matrix is composed of ≈90 wt% of PEO. Surprisingly, no oxidation peak was observed in the SITP until 5.3 V, suggesting that SITP-5 achieves a wider ESW. The improved electrochemical stability of SITP over a wide range of voltages suggests that it will match well with high-voltage cathode materials. We hypothesized that this result can be attributed to the polybutylene terephthalate (PBT) block in Poly Active, which is supposed to be highly oxidative stable, and thus succeeds in improving the overall electrochemical stability of the SITP with only 10 wt% content.

This eliminates the need to introduce the aforementioned inorganic fillers into the SITP, avoiding cost escalation and possible interfacial incompatibility (at the interface between polymer matrix and inorganic fillers) and maintaining structural integrity. For instance, the semi-interpenetrating network can exhibit a nearly unchanged ionic conductivity when subjected to repetitive mechanical stretching (Figure S17 and Note S14, Supporting Information). Notably, the ionic conductivity of SITP-5 is close to that of stretchable gel polymer electrolytes (GPEs), whose high ionic conductivities are enabled by plasticizers or other liquid components.[11] This result suggests that SITP has potential for application in flexible ionic conductors.

We compare the electrochemical properties of SITP with those of state-of-the-art solid electrolytes. As shown in Figure 3g, SITP-5 exhibits a high ESW of 5.3 V and a high ionic conductivity of 0.68 mS cm^{-1} at elevated temperatures. This result is superior to most solid electrolytes reported in the literature (see Table S3, Supporting Information) and positions SITP-5 in the upper right of the figure. Table S4 (Supporting Information) further shows that the ionic conductivity of SITP-5 at room temperature is as high as 0.11 mS cm^{-1}, which is only lower than some electrolytes containing inorganic fillers such as $LiZr_2(PO_4)$ (entry 9) or plasticizers such as low molecular weight PEO (entry 30). However, its ESW is higher than both electrolytes. What's more, Figure 3h shows the t_+ and σ_+ of the SITP compared to state-of-the-art solid electrolytes. SITP-5 has a t_+ of 0.51 at 80 °C. Combined with its high ionic conductivity of 1.03 mS cm^{-1}, SITP-5 can exhibit a high σ_+ of 0.53 mS cm^{-1}, which is even higher than that of single ion electrolytes possessing a high t_+ (>0.9) but lower σ (<0.4 mS cm^{-1}). At ambient temperature, SITP-5 also exhibits a relatively high σ_+ value of 0.065 mS cm^{-1}. It is noteworthy that a CPE (PEO-UIO66) has a higher σ_+, which can be attributed to the presence of a liquid plasticizer in its MOF particles (Table S4, Supporting Information).

2.4. Electrochemical Performance of the $LiFePO_4$/SITP-5/Li Cell

Finally, the SITP-5 was used to assemble an all-solid-state $LiFePO_4$/SITP-5/Li cell, which consisted of a Li anode and a LiFePO4 cathode. As shown in **Figure 4**, we tested the electrochemical performance of the cell at different charging/discharging current rates at 50 °C. The flat voltage plateaus shown in Figure 4a are related to the redox couple reaction on the cathode between Fe^{3+}/Fe^{2+}, which maintained a consistent value at ≈3.4 V (0.05 C), demonstrating the lower overpotential of the electrodes with the SITP-5 solid polymer electrolyte and good conductivity of SITP. With the high current rate (Figure 4b), the cell was still able to achieve a low overpotential, indicating both the impressive ionic conductivities of SITP and the good compatibility between the electrolyte and electrode materials.[55] The charge and discharge capacities and coulombic efficiency of the cells as a function of cycle number are presented in Figure 4c. When the cells were tested at various current rates measurement, the discharge capacities of the $LiFePO_4$/SITP-5/Li cell were obtained with 170.4, 161.3, 156.4, 145.5, and 125.0 mAh g^{-1} at rates of 0.05 C, 0.1 C, 0.2 C, 0.5 C, and 1 C, respectively. These values are close to the theoretical discharge capacity of $LiFePO_4$ (174 mAh g^{-1}).[54] The coulombic efficiency in the first

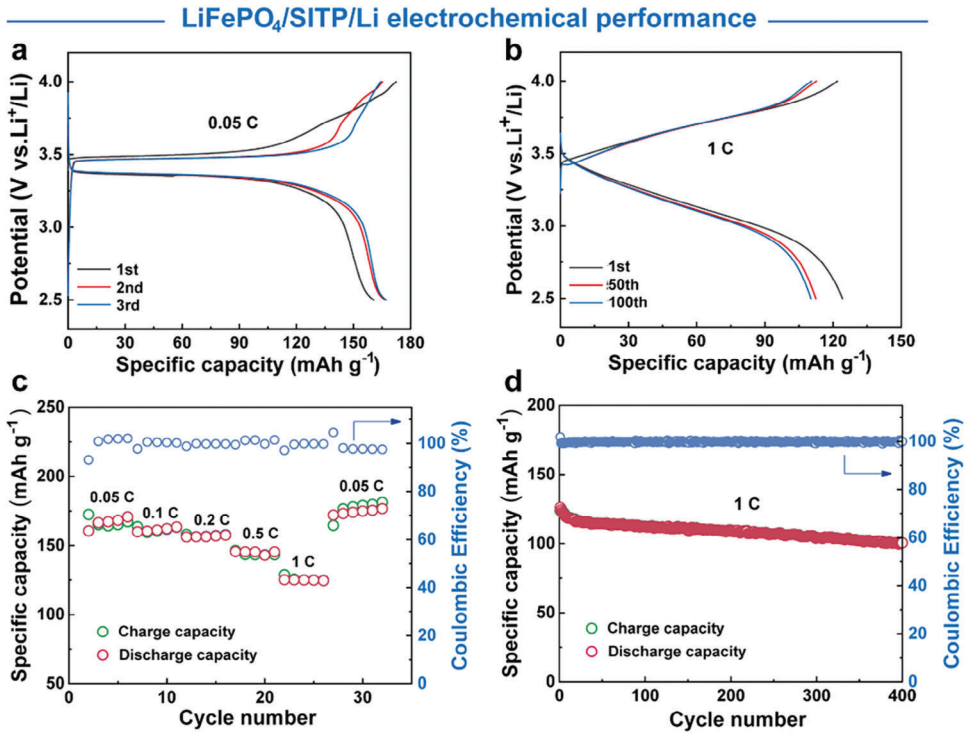

Figure 4. Electrochemical performance of the $LiFePO_4$/SITP-5/Li cell after polarization at 50 °C. a,b) Galvanostatic discharge–charge curves of the cell cycle at 0.05 C and 1 C, respectively. c) Rate capability of the cell. d) Long-term cycling of the cell cycled at 1 C.

cycle is 93.1% and almost maintains at more than 98% for subsequent cycles. The low efficiency for the first cycle is possibly due to an initial poor interfacial contact between the polymer electrolyte film and $LiFeO_4$ electrode which improves after the first cycle. This result is also comparable to other SPEs or CPEs containing inorganic fillers, demonstrating the ability of our SITP to compete with state-of-the-art solid electrolytes. The long-term cycling performance results (Figure 4d) show that after 400 cycling tests, the cell still maintained the high discharge capacity of 100 mAh h^{-1}, verifying the robustness of the SITP-5. The decrease in capacity with increasing cycle numbers mostly comes from an increase in contact resistance during cycling, a phenomenon that is observed in most SPE systems.[56,57]

3. Conclusion

In summary, we report a new family of semi-interpenetrating dry SPEs, SITP, consisting of LiTFSI, tetra-PEO, and the alternating copolymer Poly Active. The SITPs are able to adapt to exceptionally high concentrations of lithium salt without inducing an increase in the T_g of the polymer matrix. Experimental and simulation studies indicate that the supramolecular architecture of the amorphous polymer network can simultaneously achieve a high diffusivity of the "free" charge carrier and minimize inter-chain hopping for ion migration, resulting in high ionic conductivity and a high lithium ion transfer number. The resulting SITP also exhibits excellent mechanical and electrochemical stability. This work demonstrates that by judiciously designing the supramolecular structure of the polymer matrix, unprecedented and highly promising dry SPEs are developed.

4. Experimental Section

Materials: Four-armed polyethylene glycol thiol (4arm-SH, molecular weight: 5 kDa) was purchased from Jenkem Technology USA. Linear PEG diacrylate (PEGDA, average molecular weights: 250 or 2000 Da), linear PEO (average molecular weights: 5 kDa), lithium bis(trifluoromethane sulfonyl) imide (LiTFSI, 99.95%), and 2,2-dimethoxy-2-phenyl acetophenone (DMPA, 99%) were purchased from Merck. PolyActive (1500PEOT77PBT23) was purchased from PolyVation BV. Lithium plates were purchased from Shenzhen D.X. Technology and stored in a glove box. AR grade solvents were purchased from Chem-Supply. Anhydrous tetrahydrofuran (THF) was obtained using a benzophenone/ketyl still. All other materials were used as arrived.

Fabrications of SITP Film: In a glove box, the free-standing dry-solid polymer electrolyte SITPs (e.g., SITP-5) were synthesized as follows:[62] The PolyActive (100 mg), 4arm-SH (91 mg), PEGDA-250 Da (9.0 mg), LiTFSI (200 mg, 50 wt%) and DMPA (2.0 mg) were dissolved in 4 mL of anhydrous THF and sonicated for 20 s, affording a transparent solution (100 mg mL^{-1}). The mixture was poured into a petri dish (Φ50 × 9 mm), and the petri dish was then placed on a flat surface with a cover at R.T overnight. After the THF solvent was evaporated, the petri dish was moved into a vacuum oven (35 °C) to remove the solvent residue completely. The obtained polymer film was then irradiated under a Gel Curing UV lamp (9 × 4 W) for photoinduced "thiol-ene" cross-linking. After 4 h, the film was soaked in hexane to peel off from the petri dish. The obtained solid polymer electrolyte was stored in a vacuum desiccator for further use.

Tetra-PEO/LiTFSI films were fabricated via the same procedure except that PolyActive was not added.

By adjusting the feeding ratio of LiTFSI and polymer precursors, SITPs, and tetra-PEO/LiTFSI films with different LiTFSI, PolyActive, or Tetra-PEO weight loading were synthesized via the same method. The thickness of the dry-SPE films was in the range of 120–150 µm.

Engineering plastics Pebax 2533 and 1657 were also introduced into tetra-PEO as the guest polymers. However, Pebax 1657/tetra-PEO exhibits significant phase separation, and the ionic conductivity was below

10^{-5} mS cm^{-1} at 30 °C (Note S6, Supporting Information). Pebax 2533 has no common solvent with the precursors of tetra-PEO.

Fabrication of PolyActive/LiTFSI Film: The PolyActive (100 mg), linear PEO-5 kDa (100 mg), and LiTFSI (200 mg) were dissolved in 4.0 mL of anhydrous THF and sonicated for 20 s affording a transparent solution (100 mg mL^{-1}). The mixture was poured into a petri dish (Φ50 × 9 mm), and the petri dish was then placed on a flat surface with a cover at R.T. After a few hours of standing, the THF solvent evaporated, and the petri dish was moved in a vacuum oven (35 °C) to remove the THF residue fully. The film was soaked in hexane and peeled off from the petri dish. The obtained solid polymer electrolyte was stored in a vacuum desiccator.

Fabrication of PolyActive/Cross-Linked PEGDA/LiTFSI Film: The PolyActive (100 mg), PEGDA-2 kDa (100 mg), LiTFSI (200 mg), and DMPA (2.0 mg) were dissolved in 4 mL of anhydrous THF and sonicated for 20 s, affording a transparent solution (100 mg mL^{-1}). The mixture was poured into a petri dish (Φ50 × 9 mm), and the petri dish was then placed on a flat surface with a cover at R.T. After a few hours of standing, the THF solvent evaporated, and the petri dish was moved in a vacuum oven (35 °C) to remove the THF residue fully. The Gel Curing UV lamp (9 × 4 W) was then switched "on", and the photoinduced polymerization was carried out in the oven under a low vacuum (0.1 atm). After another 4 h, the film was soaked in hexane and peeled off from the petri dish. The obtained solid polymer electrolyte was stored in a vacuum desiccator.

Characterizations: X-ray photoelectron spectroscopy (XPS) analysis was performed on a VG ESCALAB 220i-XL spectrometer under an ultra-high vacuum (6×10^{-9} mbar).

UV–vis spectroscopy measurement was carried out on a Shimadzu UV–vis Spectrophotometer.

The attenuated total reflectance-Fourier transform infrared (ATR-FTIR) spectra were measured on a Bruker Alpha II spectrometer.

Scanning electrode microscopy (SEM) images were captured on an FEI Quanta 200 ESEM FEG microscope. Samples were pre-coated with gold using a Dynavac Mini Sputter Coater before imaging.

Pulsed-field gradient nuclear magnetic resonance (PFG-NMR) was performed on a Bruker 300 MHz Avance III wide-bore spectrometer equipped with a Diff50 probe. The maximum gradient strength of the probe was 2900 G cm^{-1}. The samples were first packed into 4 mm ZrO_2 magic angle spinning rotors in an argon-filled glove box and sealed with an air-tight cap. The rotors were then transferred out of the glovebox and inserted into a 5 mm glass NMR tube for diffusion measurements. A stimulated echo pulse sequence was used to record the diffusion coefficients. The diffusion time was 100 ms for both ^{7}Li and ^{19}F. The gradient pulse duration was 5 ms. Gradient strength was varied between 0.5 and 2700G cm^{-1} at 32 steps on a log scale. The recycle delay was 2 s for both nuclei.

Raman spectra were recorded using a Renishaw inVia system with a 532 nm laser beam.

Differential Scanning Calorimeter (DSC) profiles were recorded by a Perkin Elmer LAB SYS-DSC 8500 in the temperature range from −65 to 100 °C.

Mechanical elastic tests were performed on an Instron 5944 Microtester at room temperature. All samples were cast into 20 mm × 50 mm × 0.5 mm strips for testing.

Positron annihilation lifetime spectroscopy (PALS) measurements were performed on an EG&G Ortec fast–fast coincidence spectrometer. The samples were stacked to 2 mm thick on each side of a Mylar sealed $^{22}NaCl$ point source (1.5×10^{6} Bq) under vacuum (1×10^{-6} torr). The fraction-free volume was calculated according to the methods reported elsewhere.[58]

Electrochemical Measurements: All electrochemical performance of the dry-SPEs was measured using an electrochemical workstation (Biologic VSP-300).

The ionic conductivity of the dry-solid polymer electrolytes (SPEs) was determined by the Electrochemical Impedance Spectroscopy (EIS) technique in the frequency range from 7×10^{6} to 0.1 Hz with the amplitude of 10 mV, at a temperature range from 20 to 80 °C. The freestanding dry-SPEs films (Φ12 mm) were sandwiched in between two stainless steel (SS) disks as blocking electrodes [SS | dry-SPE | SS] with a 120 µm Teflon O-ring spacer and assembled into a coin cell in an argon-filled glove box. Before measurements, all the samples were dried in a vacuum at 50 °C for 48 h and stored in an argon-filled glovebox (H_2O <0.1 ppm) to exclude any solvent effects. All the measurements were performed in a sealed oven with a humidity degree below 5%. The ionic conductivities of the dry-SPEs were acquired by fitting their Nyquist plots using the following equivalent circuit:[59]

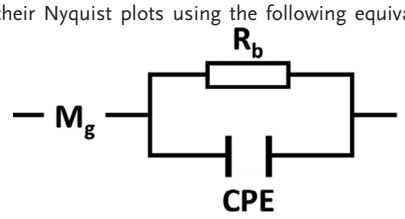

The stretch-dependent ionic conductivities of SITP-5 were measured using a home-made setup as follows:

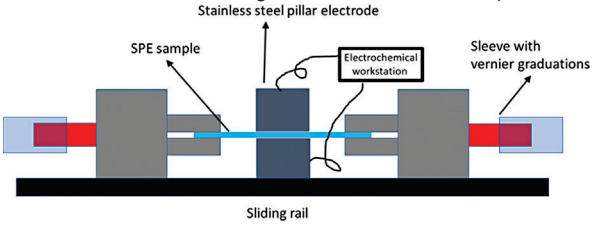

The dry-SPE film was cut into a 30 × 15 mm strip for testing. The whole setup was placed into an oven with humidity below 5% and 20 °C. The ionic resistance was measured by EIS, and the thickness of the dry-SPE film was measured each time before EIS testing to calculate ionic conductivity. With the elongation of the dry-SPE film, the thickness of the dry-SPE film was reduced to 92 ± 1% of the original value at the stretch strain of 30%, and the width was also reduced, so the shape of the film was transformed from belt to hourglass-like.

The electrical conductivity was measured by performing chronoamperometry using [SS | dry-SPE | SS] setup with the voltage bias of 200 mV.

Molecular Dynamics Simulation: Two simplified PEO network models were designed to investigate the lithium-ion conduction mechanism with a high lithium salt concentration of [Li]: [EO] equals 0.18. Rather than using a single PEO macro-molecule in the simulation box, a smaller PEO network unit (Tetra-PEO) was used, consisting of four connected tetra-PEO structures with 20 repeat ethylene oxide units in each arm, as shown in Figure S7a (Supporting Information). The simulation box contained four Tetra-PEO macro-molecules and 233 LiTFSI. For comparison, the LiTFSI/linear PEO system (Linear PEO) was also simulated, which consists of 173 LiTFSI and 24 PEO chains with 40 EO units in each chain. Notably, tried to add two PolyActive chains into the Tetra-PEO system, which did not cause observable changes to the results.

The system was initially equilibrated at 500 K for more than 1 ns in an NPT ensemble with the Berendsen thermostat and Hoover Barostat (relaxation time was 1.0 ps for both). It was cooled down to 393–353 K and equilibrated for more than 2 ns using the Nose–Hoover thermostat and Hoover Barostat with a relaxation constant of 5.0 and 10.0 ps for each, respectively until the system reached equilibrium, i.e., energy and volume become constant. Then the system was run in an NVE ensemble for 10–20 ns to collect trajectory files for dynamics analysis. The pressure was set to 1.0 atm. The 1 and 2 fs time steps were adopted for NPT and NVE calculation, respectively. The SHAKE algorithm was used for bond constraint with a shake tolerance of 1.0×10^{-6} when a 2 fs time step was used. A cut-off of 12 Å was adopted for both the Van der Waals force and the real space of Ewald. The Velocity Verlet integration algorithm was used. The Ewald summation method with a precision of 1×10^{-6} was adopted to treat Coulomb interaction in a periodic system. A uniform scale factor of 0.7 was adopted to scale down the net atomic charge for Li^{+} and $TFSI^{-}$.

The energy potential of ions was described by the OPLS_AA force field. The parameters for Li^+ and $TFSI^-$ were all taken from the CL&P force field,[60] which was developed based on the same potential function of OPLS_AA. The force field parameters of PEO were generated based on the LigParGen force field generator,[61] and the atomic charge has been slow Lightly modified so that the structurally equivalent atoms carry the same charge.

Assembly of LiFePO4/SITP-5/Li Cell: $LiFePO_4$ was mixed with Super-P and PVDF to afford the cathode slurry under the ratio of LFP: Super-P: PVDF = 8:1:1 using NMP as solvent. The cathode slurry was then coated on carbon-coated Al foil, drying at 110 °C overnight before use. The electrode was punched into circles with 8 mm in diameter, and LFP loading was ≈1.4 mg cm^{-2}. The lithium metal was employed as an anode. Dimethyl carbonate (DMC) (5 uL) was added to SITP-5 for battery assembly. The assembled cell was heated at 80 °C for 3 days before testing at 50 °C. For battery measurement, the 1 C rate was determined to be 170 mAh g^{-1} for LFP cathode.

Supporting Information

Supporting Information is available from the Wiley Online Library or from the author.

Acknowledgements

Q.F. acknowledges the Australian Research Council (ARC) under the Future Fellowship (FT180100312). F.C. acknowledges the Australian Research Council for funding via the Australian Centre for Electro materials Science (CE140100012) and computational resources provided at the NCI National Facility systems at the Australian National University through the National Computational Merit Allocation Scheme supported by the Australian Government. Q. Liang acknowledges the financial support from the ARC (DE190100445). D.L. was grateful for the financial support from the ARC (FL180100029) and the University of Melbourne.

Conflict of Interest

The authors declare no conflict of interest.

Data Availability Statement

The data that support the findings of this study are available from the corresponding author upon reasonable request.

Keywords

electrochemical stability window, ionic conductivity, solid-state electrolyte, supramolecular architecture, transference number, Vogel–Tammann–Fulcher theory

Received: December 5, 2023
Published online:

[1] X. Li, L. Zhang, B. Wang, G. Xu, S. Yu, M. Pan, S. Dou, Y. Li, J. Zhao, *Electrochim. Acta* **2020**, *332*, 135357.
[2] C. Keplinger, J.-Y. Sun, C. C. Foo, P. Rothemund, G. M. Whitesides, Z. Suo, *Science* **2013**, *341*, 984.
[3] J.-Y. Sun, C. Keplinger, G. M. Whitesides, Z. Suo, *Adv. Mater.* **2014**, *26*, 7608.
[4] C.-C. Kim, H.-H. Lee, K. H. Oh, J.-Y. Sun, *Science* **2016**, *353*, 682.
[5] H. J. Kim, B. Chen, Z. Suo, R. C. Hayward, *Science* **2020**, *776*, 773.
[6] C. Yang, Z. Suo, *Nat. Rev. Mater.* **2018**, *3*, 125.
[7] A. X. Chen, A. T. Kleinschmidt, K. Choudhary, D. J. Lipomi, *Chem. Mater.* **2020**, *32*, 7582.
[8] D. G. Mackanic, X. Yan, Q. Zhang, N. Matsuhisa, Z. Yu, Y. Jiang, T. Manika, J. Lopez, H. Yan, K. Liu, X. Chen, Y. Cui, Z. Bao, *Nat. Commun.* **2019**, *10*, 5384.
[9] Y. Zhao, L. Wang, Y. Zhou, Z. Liang, N. Tavajohi, B. Li, T. Li, *Adv. Sci.* **2021**, *8*, 2003675.
[10] Y. Jiang, X. Yan, Z. Ma, P. Mei, W. Xiao, Q. You, Y. Zhang, *Polymers* **2018**, *10*, 1237.
[11] Z. Xue, D. He, X. Xie, *J. Mater. Chem. A* **2015**, *3*, 19218.
[12] M. Chintapalli, K. Timachova, K. R. Olson, S. J. Mecham, D. Devaux, J. M. Desimone, N. P. Balsara, *Macromolecules* **2016**, *49*, 3508.
[13] M. Martinez-Ibañez, E. Sanchez-Diez, L. Qiao, Y. Zhang, X. Judez, A. Santiago, I. Aldalur, J. Carrasco, H. Zhu, M. Forsyth, M. Armand, H. Zhang, *Adv. Funct. Mater.* **2020**, *30*, 2000455.
[14] X. Wang, F. Chen, G. M. A. Girard, H. Zhu, D. R. Macfarlane, D. Mecerreyes, M. Armand, P. C. Howlett, M. Forsyth, *Joule* **2019**, *3*, 2687.
[15] K. M. Diederichsen, H. G. Buss, B. D. Mccloskey, *Macromolecules* **2017**, *50*, 3831.
[16] Y. Tominaga, K. Yamazaki, *Chem. Commun.* **2014**, *50*, 4448.
[17] D. J. Brooks, B. V. Merinov, W. A. Goddard, B. Kozinsky, J. Mailoa, *Macromolecules* **2018**, *51*, 8987.
[18] N. Hasan, M. Pulst, M. H. Samiullah, J. Kressler, *J. Polym. Sci., Part B: Polym. Phys.* **2019**, *57*, 21.
[19] D. Diddens, A. Heuer, O. Borodin, *Macromolecules* **2010**, *43*, 2028.
[20] H. Zhang, C. Li, M. Piszcz, E. Coya, T. Rojo, L. M. Rodriguez-Martinez, M. Armand, Z. Zhou, *Chem. Soc. Rev.* **2017**, *46*, 797.
[21] K. Xu, *Chem. Rev.* **2004**, *104*, 4303.
[22] J. Rolland, J. Brassinne, J.-P. Bourgeois, E. Poggi, A. Vlad, J.-F. Gohy, *J. Mater. Chem. A* **2014**, *2*, 11839.
[23] B. Kim, C.-G. Chae, Y. Satoh, T. Isono, M.-K. Ahn, C.-M. Min, J.-H. Hong, C. F. Ramirez, T. Satoh, J.-S. Lee, *Macromolecules* **2018**, *51*, 2293.
[24] Y. Matoba, Y. Ikeda, S. Kohjiya, *Solid State Ionics* **2002**, *147*, 403.
[25] Y. Tong, H. Lyu, Y. Xu, B. Prasad Thapaliya, P. Li, X.-G. Sun, S. Dai, *J. Mater. Chem. A* **2018**, *6*, 14847.
[26] J. Shim, L. Kim, H. J. Kim, D. Jeong, J. H. Lee, J.-C. Lee, *Polymer* **2017**, *122*, 222.
[27] J. Shim, K. Y. Bae, H. J. Kim, J. H. Lee, D.-G. Kim, W. Y. Yoon, J.-C. Lee, *ChemSusChem* **2015**, *8*, 4133.
[28] S. Wang, A. Wang, C. Yang, R. Gao, X. Liu, J. Chen, Z. Wang, Q. Zeng, X. Liu, H. Zhou, L. Zhang, *J. Power Sources* **2018**, *395*, 137.
[29] R. Shioiri, H. Kokubo, T. Horii, Y. Kobayashi, K. Hashimoto, K. Ueno, M. Watanabe, *Electrochim. Acta* **2019**, *298*, 866.
[30] M. A. Cabañero Martínez, N. Boaretto, A. J. Naylor, F. Alcaide, G. D. Salian, F. Palombarini, E. Ayerbe, M. Borras, M. Casas-Cabanas, *Adv. Energy Mater.* **2022**, *12*, 2201264.
[31] J. Wang, S. Li, Q. Zhao, C. Song, Z. Xue, *Adv. Funct. Mater.* **2021**, *31*, 2008208.
[32] X. Liu, G. Ding, X. Zhou, S. Li, W. He, J. Chai, C. Pang, Z. Liu, G. Cui, *J. Mater. Chem. A* **2017**, *5*, 11124.
[33] Q. Zhou, J. Ma, S. Dong, X. Li, G. Cui, *Adv. Mater.* **2019**, *31*, 1902029.
[34] K. Hatakeyama-Sato, T. Tezuka, M. Umeki, K. Oyaizu, *J. Am. Chem. Soc.* **2020**, *142*, 3301.
[35] D. Lin, W. Liu, Y. Liu, H. R. Lee, P.-C. Hsu, K. Liu, Y. Cui, *Nano Lett.* **2016**, *16*, 459.

[36] T. Sakai, T. Matsunaga, Y. Yamamoto, C. Ito, R. Yoshida, S. Suzuki, N. Sasaki, M. Shibayama, U.-I. Chung, *Macromolecules* **2008**, *41*, 5379.
[37] M. Shibayama, X. Li, T. Sakai, *Colloid Polym. Sci.* **2019**, *297*, 1.
[38] S. S. Sheiko, A. V. Dobrynin, *Macromolecules* **2019**, *52*, 7531.
[39] H. Kamata, Y. Akagi, Y. Kayasuga-Kariya, U.-I. Chung, T. Sakai, *Science* **2014**, *343*, 873.
[40] M. Tosa, K. Hashimoto, H. Kokubo, K. Ueno, M. Watanabe, *Soft Matter* **2020**, *16*, 4290.
[41] L. Long, S. Wang, M. Xiao, Y. Meng, *J. Mater. Chem. A* **2016**, *4*, 10038.
[42] W. Gorecki, M. Jeannin, E. Belorizky, C. Roux, M. Armand, *J. Phys. Condens. Matter* **1995**, *7*, 6823.
[43] N. A. Stolwijk, C. Heddier, M. Reschke, M. Wiencierz, J. Bokeloh, G. Wilde, *Macromolecules* **2013**, *46*, 8580.
[44] N. Molinari, J. P. Mailoa, B. Kozinsky, *Chem. Mater.* **2018**, *30*, 6298.
[45] D. Golodnitsky, E. Livshits, R. Kovarsky, E. Peled, S. H. Chung, S. Suarez, S. G. Greenbaum, *Electrochem. Solid-State Lett.* **2004**, *7*, A412.
[46] E. Livshits, R. Kovarsky, N. Lavie, Y. Hayashi, D. Golodnitsky, E. Peled, *Electrochim. Acta.* **2005**, *50*, 3805.
[47] M. Echeverri, C. Hamad, T. Kyu, *Solid State Ionics* **2014**, *254*, 92.
[48] Q. Zhao, C. Shen, K. P. Halloran, C. M. Evans, *ACS Macro Lett.* **2019**, *8*, 658.
[49] A. Nguyen, T. C. Rhoades, R. D. Johnson, K. M. Miller, *Macromol. Chem. Phys.* **2017**, *218*, 1700337.
[50] G. Zardalidis, A. Pipertzis, G. Mountrichas, S. Pispas, M. Mezger, G. Floudas, *Macromolecules* **2016**, *49*, 2679.
[51] Y.-C. Jung, S.-M. Lee, J.-H. Choi, S. S. Jang, D.-W. Kim, *J. Electrochem. Soc.* **2015**, *162*, A704.
[52] K. Liu, X. Li, J. Cai, Z. Yang, Z. Chen, B. Key, Z. Zhang, T. L. Dzwiniel, C. Liao, *ACS Energy Lett.* **2021**, *6*, 1315.
[53] H. Zhang, X. An, Y. Long, H. Cao, Z. Cheng, H. Liu, Y. Ni, *Chem. Eng. J.* **2021**, *425*, 130632.
[54] B. Lung-Hao Hu, F.-Y. Wu, C.-T. Lin, A. N. Khlobystov, L.-J. Li, *Nat. Commun.* **2013**, *4*, 1687.
[55] X. Wang, H. Zhai, B. Qie, Q. Cheng, A. Li, J. Borovilas, B. Xu, C. Shi, T. Jin, X. Liao, Y. Li, X. He, S. Du, Y. Fu, M. Dontigny, K. Zaghib, Y. Yang, *Nano Energy* **2019**, *60*, 205.
[56] S.-T. Hsu, B. T. Tran, R. Subramani, H. T. T. Nguyen, A. Rajamani, M.-Y. Lee, S.-S. Hou, Y.-L. Lee, H. Teng, *J. Power Sources* **2020**, *449*, 227518.
[57] J. Zheng, C. Sun, Z. Wang, S. Liu, B. An, Z. Sun, F. Li, *Angew. Chem.* **2021**, *133*, 18596.
[58] W. Xie, H. Ju, G. M. Geise, B. D. Freeman, J. I. Mardel, A. J. Hill, J. E. Mcgrath, *Macromolecules* **2011**, *44*, 4428.
[59] J. Bae, Y. Li, J. Zhang, X. Zhou, F. Zhao, Y. Shi, J. B. Goodenough, G. Yu, *Angew. Chem. Int. Ed.* **2018**, *57*, 2096.
[60] J. N. Canongia Lopes, A. A. H. Pádua, *Theor. Chem. Acc.* **2012**, *131*, 1129.
[61] L. S. Dodda, I. Cabeza De Vaca, J. Tirado-Rives, W. L. Jorgensen, *Nucleic Acids Res.* **2017**, *45*, W331.
[62] X. Wang, G. M. A. Girard, H. Zhu, R. Yunis, D. R. Macfarlane, D. Mecerreyes, A. J. Bhattacharyya, P. C. Howlett, M. Forsyth, M. Forsyth, *ACS Appl. Energy Mater.* **2019**, *2*, 6237.